*Journal of Power Sources*, 8 (1982) 159 - 173



# SULFATE PASSIVATION IN THE LEAD–ACID SYSTEM AS A CAPACITY LIMITING PROCESS

W. KAPPUS and A. WINSEL

*VARTA Batterie AG, Forschungs- und Entwicklungszentrum, Gundelhardtstr. 72, D-6233 Kelkheim/Ts. (F.R.G.)*

## Summary

Calculations of the discharge capacity of Pb and $PbO_2$ electrodes as a function of various parameters are presented. They are based on the solution–precipitation mechanism for the discharge reaction and its formulation by Winsel *et al.* A logarithmic pore size distribution is used to fit experimental porosigrams of Pb and $PbO_2$ electrodes. Based on this pore size distribution the capacity is calculated as a function of current, BET surface, and porosity of the $PbSO_4$ diaphragm. The $PbSO_4$ supersaturation as the driving force of the diffusive transport is chosen as a free parameter.

## 1. Introduction

In the course of our ILZRO sponsored research program on the theory of the lead–acid cell we have investigated two basic questions:

— which factors determine the electrode capacity and what are the functional dependencies [1 - 3];

— which factors determine the structure transformations during cycling and what are the underlying laws [4].

It became evident from our investigations that the electrode evaluation using the flow-through method [5] is a powerful tool for basic research on lead–acid cells. It furthermore became clear that the lead–acid cell is a system with strong interrelations and feed back loops which make it necessary to study in detail any step of a cycle and its consequences on the transformation process.

Though our theoretical research led to useful models there was still a lack of understanding of some of our previous experimental results [1, 2]. We have therefore worked out a theory for $PbSO_4$ passivation on the basis of the model of Winsel *et al.* [6]. Assuming a rather realistic pore size distribution we were able to fit experimental findings to a satisfactory extent and to deduce some relations of fundamental interest.

0378-7753/82/0000-0000/$02.75 

## 2. The passivation model of flow-through electrodes

### *2.1. Introduction*

Four different processes are known to determine the capacity of the positive and of the negative electrodes of the lead–acid accumulator, each of which may become dominant under certain conditions [7, 8]. These are outlined as follows:

(i) Due to the fact that the sulfuric acid is consumed by the discharge reaction in the positive as well as in the negative electrode, the electrolyte concentration within the pore system decreases and limits the capacity by pauperization [9]. Therefore the electrodes of the different types of accumulators are designed with regard to their thickness in such a way that during the usual discharge time the electrolyte may diffuse sufficiently quickly from the electrolyte space between the electrodes into the entire pore system.

(ii) At very low discharge currents when the electrolyte concentration within the pores is always established by diffusion from outside the electrodes, the electronic conductivity of the active material disappears by the conversion of conductive lead or lead dioxide into non-conductive lead sulfate [10]. The capacity at which this occurs gives an ultimate value for the material utilization under normal conditions.

It is well known however that in positive electrodes which are constructed from antimony-free or low antimony content grids the capacity very often exhibits a collapse after some quick and deep cycles. This so-called "antimony-free effect" is caused by an early loss of the electronic conductivity of the active material in the region of the grid, due to a changed current distribution which, from cycle to cycle, increasingly favours the near-grid region and leaves the more distant material partly undischarged.

(iii) Crystals of lead sulfate are formed by the discharge reaction and act as a diaphragm in front of the inner surface of the active material. This diaphragm limits the diffusion of divalent lead ions from the electrode surface (where they have been formed) into the entire pore solution, thus blocking the discharge reaction. This process is called "sulfate passivation" and is of great importance when, during discharge, the electrolyte is forced to flow through the pore system. Furthermore, in very small pores the reaction product may fill the pore volume completely, thus limiting the capacity [6]. Additionally, a current distribution which is not homogeneous over the electrode thickness may result in a $PbSO_4$ diaphragm at the geometric surface of the electrode which also leads to a capacity limit [11].

(iv) If a lead–acid cell is discharged at low temperature under cold cranking conditions ice crystals are formed within the pore solution. This happens when, due to the discharge reaction, the acid concentration decreases below the freezing point of the electrolyte. These ice crystals form a diaphragm in front of the electrode/electrolyte interface. This hinders the diffusion of divalent lead ions away from the surface into the pore-

electrolyte where they form lead sulfate crystals. This process is called "ice passivation" and is very closely related to sulfate passivation [6]. A theory for the lead sulfate passivation model was given by Winsel, Hullmeine and Voss (WHV) [6] and applied to positive and negative electrodes under cold cranking conditions.

In the present paper we shall apply the formalism given by the aforementioned authors (WHV) to an artificial lead electrode and to an artificial lead dioxide electrode. We shall use the same nomenclature as WHV and denote their formula [6] as WHV.

*2.2. A short review of the theory [6]*

During the discharge of an electrode, passivating layers of $PbSO_4$ are formed by a solution/precipitation mechanism [12]. These layers form a diaphragm of mostly well defined crystals. The diaphragm contributes to the internal resistance. It affects the diffusion of acid molecules to the electrode/electrolyte interface and it hinders the diffusion of the divalent lead ions formed away from this interface. This last mentioned effect is the most important one because it leads to a limiting current behaviour which determines the capacity.

By theory it is postulated that the contribution of a given pore to the current is terminated when the pore volume is completely filled with the reaction product or when the current density at the inner surface becomes equal to the (decreasing) limiting current density of the diffusion of $Pb^{2+}$ through the passivating diaphragm. Two assumptions are basic to the theory, first a homogeneous current density over the active inner surface, and second the absence of any mass transfer between different pores.

In the following section WHVs results are applied to positive and negative electrodes using a realistic model of the pore distribution function which governs the details of the pore filling process. Functional dependencies of the electrode capacity from various parameters are presented.

*2.3. Definition of the artificial electrodes*

In our treatment both positive and negative electrodes are defined by the same type of distribution function of the specific pore volume $V(r)$ as a function of the pore radius $r$:

$$V(r) = V_P/r \ln(r_2/r_1); \qquad r_1 \leqq r \leqq r_2 \tag{1}$$
$$= 0; \qquad r > r_2, \; r < r_1.$$

Simultaneously function (1) defines the distribution function of the specific length $l(r)$ of the pores due to WHV (2)

$$l(r) = V_P/\pi r^3 \ln(r_2/r_1); \qquad r_1 \leqq r \leqq r_2 \tag{2}$$
$$= 0; \qquad r < r_1, \; r > r_2$$

and of the specific surface of the pores $O(r)$ due to WHV (4)

$$O(r) = 2V_P/r^2 \ln(r_2/r_1); \qquad r_1 \leqq r \leqq r_2 \tag{3}$$
$$= 0\ ; \qquad r < r_1\ ,\ r > r_2.$$

By integration of the preceding functions we get the corresponding accumulated functions as follows:

$$W(r) = \int_0^r V(r)\mathrm{d}r \tag{4}$$

$$W(r)\begin{cases} = 0; & 0 < r < r_1 \\ = V_P \ln(r/r_1)/\ln(r_2/r_1); & r_1 \leqq r \leqq r_2 \\ = V_P; & r > r_2. \end{cases} \tag{5}$$

$W(r)$ defines the pore volume per unit of active material of all pores with radii smaller than $r$. In the same way we get the internal surface area $S(r)$ per unit of active material of all pores with radii smaller than $r$ by integration of eqn. (3):

$$S(r) = \int_0^r O(r)\mathrm{d}r \tag{6}$$

$$S(r)\begin{cases} = 0; & 0 < r < r_1 \\ = 2V_P(1/r_1 - 1/r)/\ln(r_2/r_1); & r_1 \leqq r \leqq r_2 \\ = 2V_P(1/r_1 - 1/r_2)/\ln(r_2/r_1); & r > r_2 \end{cases} \tag{7}$$

$$S_0 = S(r_2). \tag{8}$$

The function $W(r)$ in eqn. (5) is a realistic approximation of distribution functions as they are often measured by porosimetric methods. Figure 1(a) gives an example for a negative, Fig. 1(b) for a positive electrode. The BET-surface $S_0$ for an electrode according to our model can be calculated from eqn. (8) if $V_P$, $r_1$ and $r_2$ are given. So we can take experimental values for $V_P$, fix a value for $r_2$ and adapt $r_1$ in such a way that the calculated BET-surface fits the experimental findings.

At a given specific current the electrode potential collapses due to sulfate passivation after a time $t^*$. When this happens, all pores having radii smaller than $r_{t*}$ are completely filled with the reaction product, $PbSO_4$. The theory defines this boundary radius $r_{t*}$ by formula WHV (4) which reads as follows:

$$\int_{r_{t*}}^{\infty} O(r)\mathrm{d}r = \lambda I r_{t*}/2P^{*2}FD\Delta c. \tag{9}$$

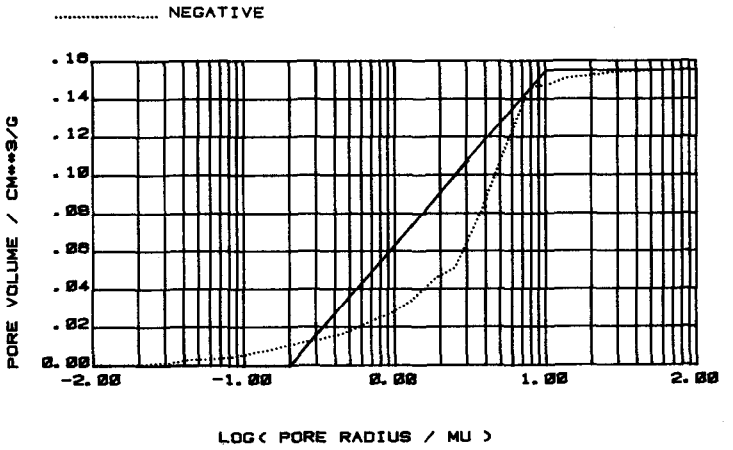


(a)

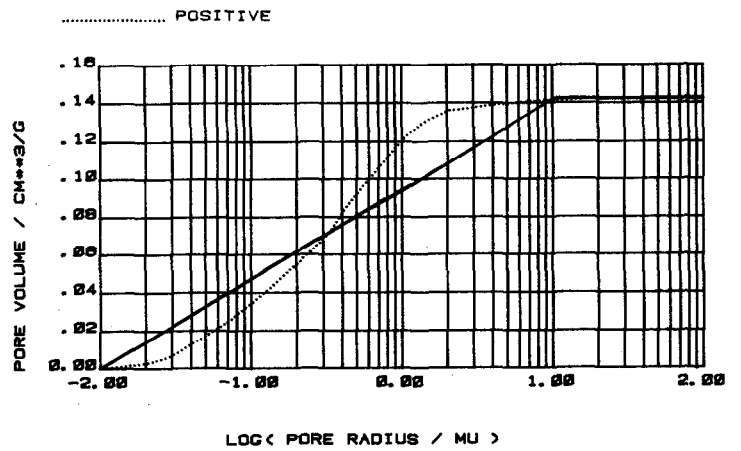


(b)

Fig. 1. Pore volume *vs.* log pore radius, measured by porosimetry, according to eqn. 5. (a) Negative electrode; (b) positive electrode.

By inserting the distribution function (3) this formula simplifies to

$$2V_P(1/r_{t^*} - 1/r_2)/\ln(r_2/r_1) = \lambda I r_{t^*}/2P^{*2}FD\Delta c. \tag{10}$$

We define an auxiliary constant $K$ by

$$K = \lambda \ln(r_2/r_1)/4P^{*2}FD\Delta c\, V_P. \tag{11}$$

Inserting this into eqn. (10) we get

$$(1/r_{t^*} - 1/r_2) = KIr_{t^*}. \tag{12}$$

By inserting the new auxiliary $x$

$$x = 2IKr_2^2 \tag{13}$$

we derive from eqn. (12) the following expression for $r_{t*}$:

$$r_{t*} = (r_2/x)(\sqrt{1+2x} - 1). \tag{14}$$

WHV (17) gives the capacity $C$ at constant specific current $I$ in terms of the boundary radius $r_{t*}$:

$$C = It^* = \frac{1}{\Delta V_0}\left\{\left[S - \int_0^{r_{t*}} O(r)\mathrm{d}r\right]\frac{r_{t*}}{2} + \int_0^{r_{t*}} V(r)\mathrm{d}r\right\}. \tag{15}$$

By inserting eqn. (14) into eqn. (15) we find the final expression for the capacity:

$$C = \frac{V_P}{\Delta V_0 \ln r_2/r_1}\left\{1 + \ln(r_2/r_1) - \frac{\sqrt{1+2x}-1}{x} + \ln\frac{\sqrt{1+2x}-1}{x}\right\}. \tag{16}$$

When all the physical constants are specified, we are able to calculate the capacity, $C$, of our artificial electrode from eqn. (16) as a function of the specific current $I$ and other parameters. We have done this calculation numerically. The results are given in Section 2.5.

*2.4. Specification of the various constants and parameters*

Table 1 lists the symbols, definitions, units and values of the different constants and parameters used in the calculations.

*2.5. The results of our calculations*

As was pointed out earlier, the boundary radius $r_{t*}$ divides the pore system into two groups: At the end of discharge at time $t^*$ all pores with radii smaller than $r_{t*}$ are completely filled with lead sulfate, whilst all pores with radii larger than $r_{t*}$ are coated with a lead sulfate diaphragm of thickness $\delta = r_{t*}/2$.

In Fig. 2(a) the logarithm of the boundary radius $r_{t*}$ is presented as a function of the specific current $I$ for different values of the dynamic supersaturation $D\Delta c$ for a negative electrode. The dotted horizontal lines show $r_1$ and $r_2$. The BET surface area is $S = 0.41$ m$^2$/g. It can be seen that the higher the current $I$ and the smaller the supersaturation concentration $\Delta c$, the smaller is the boundary radius $r_{t*}$. If, for a given dynamic supersaturation $D\Delta c$, and for a given current $I$ the calculated value of $r_{t*}$ is below $r_1$, no pores are completely filled at the end of galvanostatic discharge.

For convenience we note that 800 A/kg represents a starter current, 200 A/kg the acceleration current in electric vehicle application, and 50 A/kg heavy duty traction application.

Figure 2(b) shows the functional dependence of $r_{t*}$ for a positive electrode. The positive electrode is characterized by a smaller pore radius, $r_1$, corresponding to a higher BET surface area. The choice of the parameter range for the dynamic supersaturation $D\Delta c$ is justified by the results

TABLE 1

Symbols, definitions and values

| Symbols | Definition | Value | Unit |
|---|---|---|---|
| $F$ | Faraday constant | 26.8 | A h/mol |
| $D$ | Diffusion coefficient of $PbSO_4$ in sulfuric acid | $3.6 \times 10^{-2}$ | $cm^2/h$ |
| $\lambda$ | Tortuosity factor of the $PbSO_4$ diaphragm | 3 | 1 |
| $P^*$ | Porosity of the $PbSO_4$ diaphragm | 0.5 | 1 |
| $V_P^+$ | Specific pore volume of the positive active material | 0.14 | $cm^3/g$ |
| $V_P^-$ | Specific pore volume of the negative active material | 0.16 | $cm^3/g$ |
| $\Delta V_0^+$ | Change of volume of the positive material by discharge | 0.437 | $cm^3$/A h |
| $\Delta V_0^-$ | Change of volume of the negative material by discharge | 0.556 | $cm^3$/A h |
| $c_s$ | Saturation concentration of $PbSO_4$ in sulfuric acid of gravity 1.064 $g/cm^3$<br>of gravity 1.30 $g/cm^3$ | $2.2 \times 10^{-8}$<br>$5.02 \times 10^{-9}$ | $mol/cm^3$<br>$mol/cm^3$ |
| $r_2$ | Radius of the largest pores | $10^{-3}$ | cm |
| $r_1$ | Radius of the smallest pores | variable | cm |
| $\Delta c$ | Supersaturation concentration of $PbSO_4$ | variable | $mol/cm^3$ |
| $D\Delta c$ | Dynamic supersaturation concentration of $PbSO_4$ | variable | mol/h cm |
| $I$ | Specific current related to the mass unit of active material in completely charged state | variable | A/kg |
| $C$ | Specific capacity on galvanostatic discharge | | A h/kg |
| $t^*$ | Time until end of galvanostatic discharge | | h |
| $r_{t^*}$ | Boundary radius between completely filled and coated pores at the end of discharge | | cm |

presented in Fig. 4(b). Although the dynamic supersaturation $D\Delta c$ in the positive electrode is two orders of magnitude smaller than in the negative electrode, the complete pore filling is the prevailing limiting mechanism for the positive electrode rather than the coating mechanism.

It is instructive to see the influence of a reduced BET surface area in both cases. We have therefore plotted in Fig. 3(a) and (b) the same relations for electrodes with roughly half the BET surface area represented by an increased value of the lower characteristic radius $r_1$.

We note from a comparison of Figs. 2 and 3 that the reduced BET surface favours surface coating as the capacity limiting process. It should be mentioned that the electrodes of Fig. 2 represent the normal case, whereas

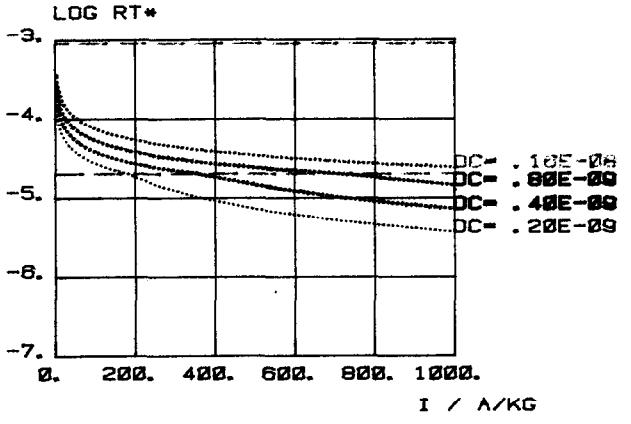


(a)

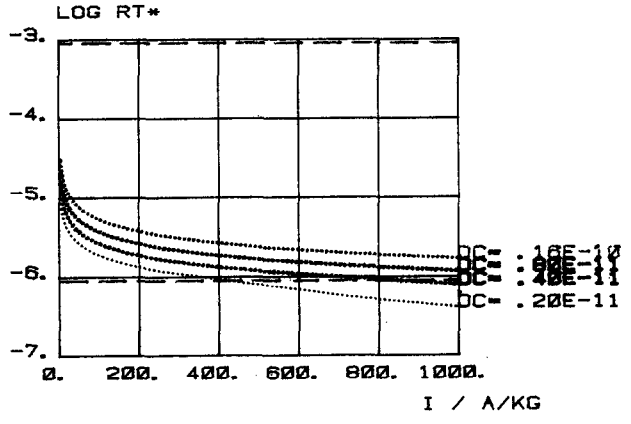


(b)

Fig. 2. Log boundary radius, $r_{t*}$, *vs.* specific current, $I$, for different values of the dynamic supersaturation $D\Delta c$. — — —, $r_1$ and $r_2$. (a) Negative electrode; (b) positive electrode.

Fig. 3 represents electrodes with bad performance due to a reduced BET surface.

Figures 4 and 5 show the capacity $C$ (active material utilization) of negative and positive electrodes as a function of the specific current $I$. The varying parameter is the dynamic supersaturation $D\Delta c$. The BET surface area corresponds to that of Fig. 2(a), (b). The broken lines represent the percolation limit (loss of conductivity) [10]. Whereas Fig. 4(a), (b) shows the current range up to 1000 A/kg, Fig. 5 (a), (b) shows only the range up to 200 A/kg.

Compared with measurements of the capacity under forced flow of electrolyte through the pore system [1, 2], the dynamic supersaturation values $D\Delta c = 8 \times 10^{-10}$ ($8 \times 10^{-12}$) for negative (positive) electrodes give the best approximation over the whole range of specific current, $I$. From this

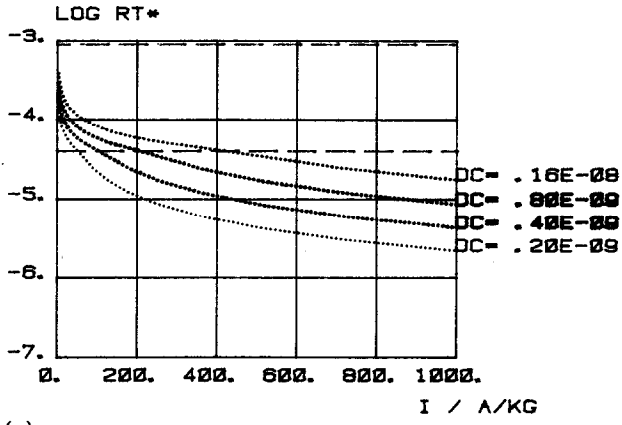


(a)

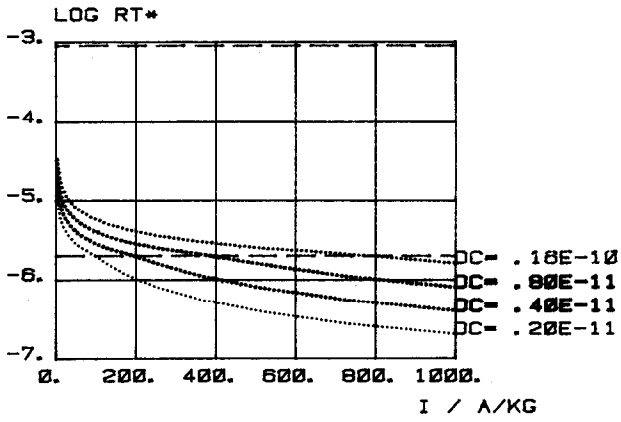


(b)

Fig. 3. As for Fig. 2, but with approximately half the BET surface area. (a) Negative electrode; (b) positive electrode.

observation we deduce that the positive electrode works with a much lower supersaturation concentration than the negative electrode. This is clearly a consequence of the smaller average pore radius, *i.e.*, the higher BET surface area of the positive electrode. The lower supersaturation in positive electrodes is thought to be one of the reasons for the high stability of the pore structure of the positive electrode during charge–discharge cycles. On the other hand, the need for an expander in the negative electrode seems to be caused by the high supersaturation with its high mass transport capability. Compared with the saturation concentration $c_s$ of $PbSO_4$ in sulfuric acid of density 1.30 g/cm$^3$ (see Table 1), we are concerned with a supersaturation of $\Delta c/c_s = 4.4$ in the case of negative electrodes and of $\Delta c/c_s = 0.044$ in the case of positive electrodes.

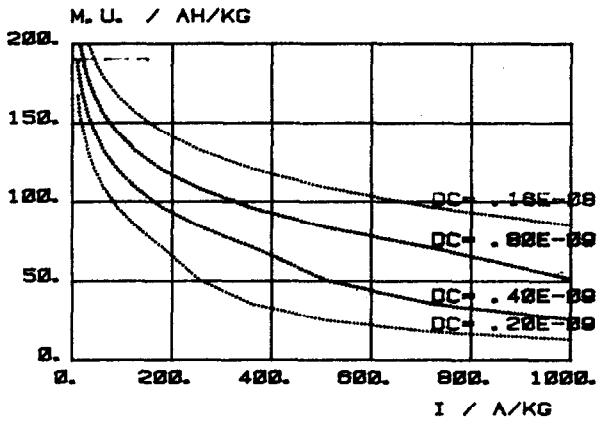


(a)

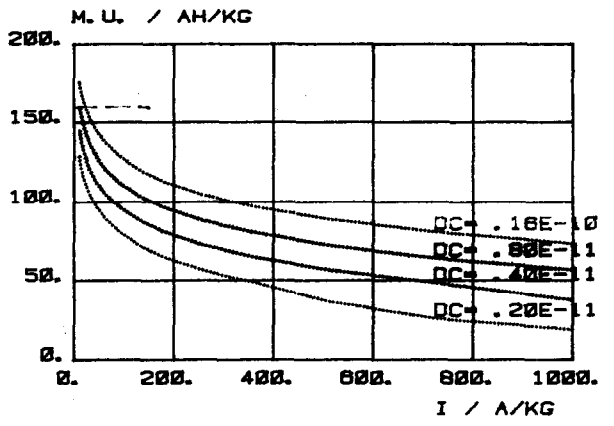


(b)

Fig. 4. Capacity, $C$, as a function of the specific current, $I$. — — —, percolation limit. (a) Negative electrode; (b) positive electrode. Current range up to 1000 A/kg.

Figures 6 and 7 show the galvanostatic capacity $C$ (active material utilization) of negative and positive electrodes as a function of the BET surface $S_0$. The varying parameter is the specific current $I$. Figures 6 and 7 differ by the dynamic supersaturation $D\Delta c$. The capacity curves show two different regions; in the low BET region a quadratic increase of $C$ is observed followed by an abrupt transition to a slow increase. This is clearly a consequence of the transition from surface coating to pore filling as the capacity determining process with increasing BET surface. The quadratic increase of the capacity with increasing BET surface has already been deduced by WHV [6] from simple arguments, and experimentally confirmed in the low temperature

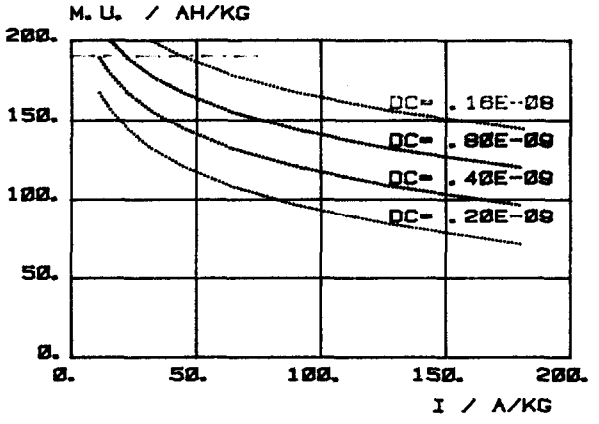


(a)

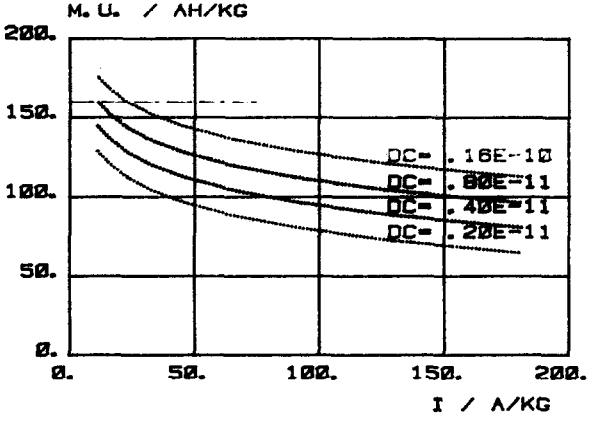


(b)

Fig. 5. Capacity, $C$, *vs.* specific current, $I$. — — —, percolation limit. (a) Negative electrode; (b) positive electrode. Current range up to 200 A/kg.

region [6]. It is interesting to note from Figs. 6(a) and 7(a) that the transition in the $C(S_0)$ slope of negative electrodes occurs in the technically important range between 0.4 and 0.6 $m^2/g$ for the starter current $I$ = 800 A/kg. Furthermore, the $C$ values roughly agree with experimental results [6]. In cold cranking applications the transition will be more drastic since pore filling by ice occurs with a larger volume change, $\Delta V_0$, than pore filling by $PbSO_4$. This matter will be discussed in more detail in another context.

Figure 8(a), (b) shows the capacity $C$ (active material utilization) as a function of the diaphragm porosity $P^*$. The varying parameter is the specific current $I$. From the definition of the auxiliary constant $K$ in eqn. (11) it can

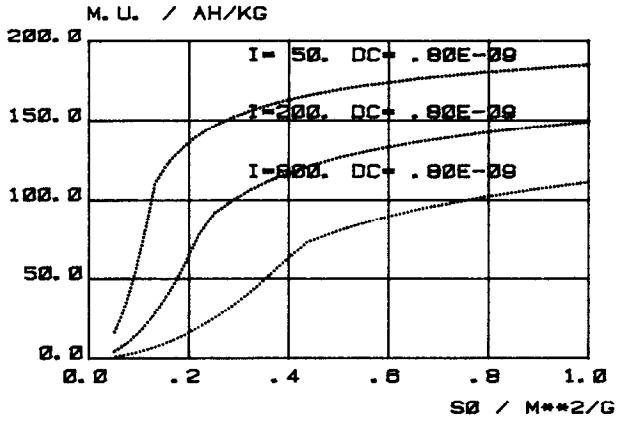


(a)

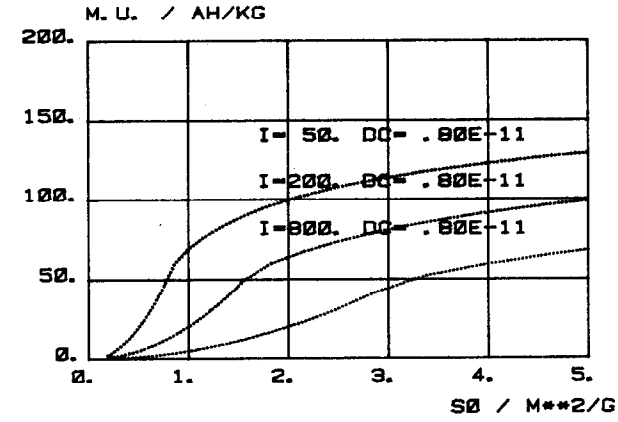


(b)

Fig. 6. Galvanostatic capacity, $C$, *vs.* BET surface, $S_0$. (a) Negative electrode; (b) positive electrode.

be seen that the variation of $P^*$ is equivalent to a quadratic variation of the dynamic supersaturation $D\Delta c$, so Fig. 8(a), (b) may also be used for demonstrating the $C(D\Delta c)$ dependency. Figure 8(a), (b) shows that the capacity is increased with increasing diaphragm porosity as is expected from the increasing transport capacity of $Pb^{2+}$ through the surface coating layer with its increasing porosity. Comparison of the capacity $C$ with experimental cold cranking capacities [6] shows that a value of $P^* = 0.5$, together with $D\Delta c = 8 \times 10^{-10}$ mole/h cm for $S_0 = 0.6$ m$^2$/g, gives a reasonable agreement between theory and experiment.

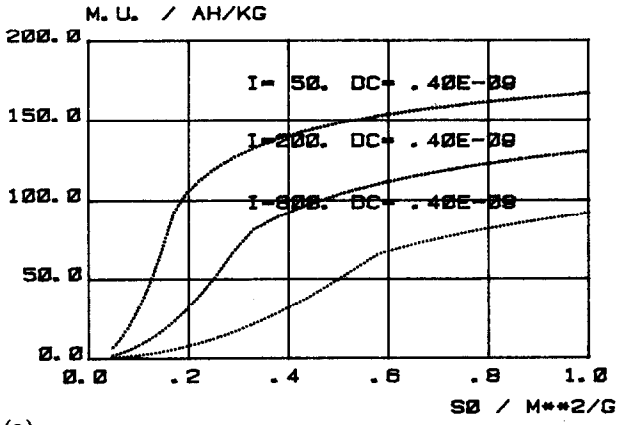


(a)

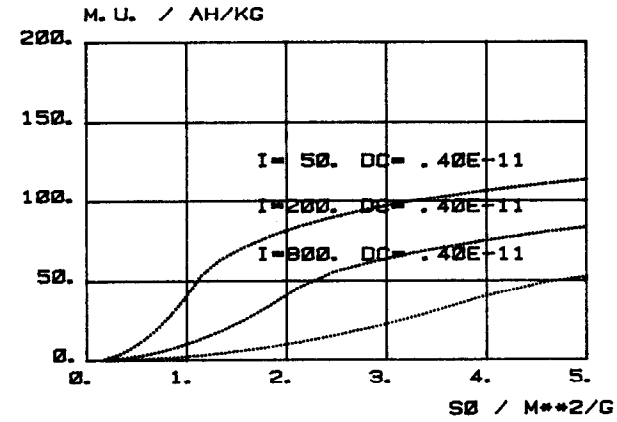


(b)

Fig. 7. Galvanostatic capacity, $C$, *vs.* BET surface, $S_0$. (a) Negative electrode; (b) positive electrode.

## 3. Conclusion

Though the calculations describe the functional relationship of the capacity of Pb and $PbO_2$ electrodes quite well, there is still a lack of understanding due to the free parameter "supersaturation". It would be desirable to find a chemical mechanism which could determine the supersaturation in the different electrodes at the end of discharge. This might be the equilibrium concentration of a basic lead sulfate covering the active surface of the electrodes, as proposed by Simon *et al.* [13] discussing a paper by Pavlov and Popova [14].

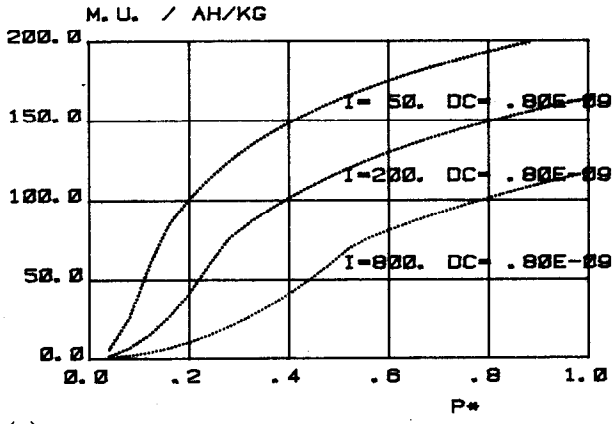


(a)

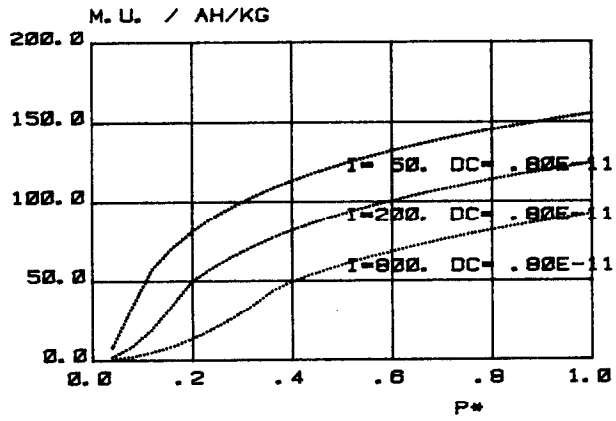


(b)

Fig. 8. Capacity $C$ (active material utilisation) *vs.* diaphragm porosity, $P^*$. (a) Negative electrode; (b) positive electrode.

Recently, Kelly *et al.* published a paper dealing with the inability of the $PbO_2$ electrode to accept recharge after deep discharge at a potential of 540 mV more negative than the rest potential of the $PbO_2$ electrode [15]. To explain their experimental results they postulate the existence of a "passivated sulfate" which cannot be oxidized to lead dioxide by the potential step technique.

In the light of our theory, the discharge capacity in their first cycle is determined by the formation of a porous lead sulfate diaphragm, as plotted in Fig. 9. The end of discharge is caused by a surface layer on the $PbO_2$ crystallites passivating the electrode. The following recharge at a high positive potential is hindered by this layer which firstly has to be removed by an autocatalytic electrochemical reaction. The increasing current which is caused by this autocatalytic process has been observed in our experiments

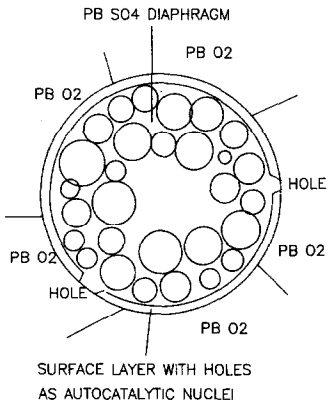


**Fig. 9. Schematic plot of a pore in a $PbO_2$ electrode with sulfate diaphragm and a surface layer with holes.**

dealing with charge acceptance of electrodes after deep discharge under flow through conditions [4].

## Acknowledgement

This work is sponsored by the International Lead Zinc Research Organization under contract No. LE-277.

## References

1 U. Hullmeine, W. Kappus, J. Schulz, E. Voss and A. Winsel, *Prog. Rep. No. 2, LE-277 ILZRO, June 1, 1978 - Dec. 31, 1978.*
2 U. Hullmeine, W. Kappus, J. Schulz, E. Voss and A. Winsel, *Prog. Rep. No. 4, LE-277 ILZRO, June 1, 1979 - Dec. 31, 1979.*
3 U. Hullmeine, W. Kappus, J. Schulz, E. Voss and A. Winsel, *Prog. Rep. No. 5, LE-277 ILZRO, Jan. 1, 1980 - May 31, 1980.*
4 U. Hullmeine, W. Kappus, E. Voss and A. Winsel, *Prog. Rep. No. 6, LE-277 ILZRO, June 1, 1980 - Dec. 31 1980.*
5 C. Liebenow, *Z. Elektrochem., 3* (1896) 71.
6 A. Winsel, U. Hullmeine and E. Voss, *J. Power Sources, 2* (1977/78) 369.
7 H. Bode, *Lead–Acid Batteries*, Wiley, New York, 1977.
8 N. A. Hampson and J. B. Lakeman, *J. Power Sources, 6* (1981) 101 - 120.
9 W. Kappus and U. Hullmeine, *Electrochim. Acta, 26* (1981) 1103.
10 H. Metzendorf, *Dissertation*, Gesamthochschule Kassel, 1980.
11 H. Bode, H. Panesar and E. Voss, *Chem. Ing. Tech., 41* (1969) 878.
12 K. J. Vetter, *Chem. Ing. Tech., 45* (1973) 213.
13 A. C. Simon, S. M. Caulder, P. J. Gurlusky and J. R. Pierson, *J. Electrochem. Soc., 121* (1974) 463.
14 D. Pavlov and R. Popova, *Electrochim. Acta, 15* (1970) 1483.
15 S. Kelly, N. A. Hampson and K. Peters, *J. Appl. Electrochem., 11* (1981) 269.